HOKKAIDO UNIVERSITY

Title	Time Change in Scale Microstructure of Fe-5 mass%Ni Alloy at 1200° C
Author(s)	Harashima, Aya; Kondo, Yasumitsu; Hayashi, Shigenari
Citation	ISIJ International, 60(2), 352-358 https://doi.org/10.2355/isijinternational.ISIJINT-2019-252
Issue Date	2020-02-15
Doc URL	https://hdl.handle.net/2115/76836
Rights	著作権は日本鉄鋼協会にある
Type	journal article
File Information	ISIJ Int. 60(2)_ 352-358 (2020).pdf



Hokkaido University Collection of Scholarly and Academic Papers : HUSCAP

ISIJ International, Vol. 60 (2020), No. 2, pp. 352–358

Time Change in Scale Microstructure of Fe-5 mass%Ni Alloy at 1 200°C

Aya HARASHIMA,[1)]* Yasumitsu KONDO[1)] and Shigenari HAYASHI[2)]

1) Process Research Laboratories, Nippon Steel Corporation, 20-1 Shintomi, Futtsu, Chiba, 293-8511 Japan.
2) Division of Materials Science and Engineering, Faculty of Engineering, Hokkaido University, Sapporo, Hokkaido, 060-8628 Japan.

(*Received on April 16, 2019; accepted on August 2, 2019; J-STAGE Advance published date: October 3, 2019*)

Ni containing steel is known to form a complex oxide scale, which consists of an outer layer of Fe-oxides and an inner layer of FeO with complicated distribution of Ni(Fe) metal particles. Due to the complex microstructure, descaling of the oxide scale formed on Ni containing steel during a hot-rolling process is very difficult. In order to improve the descaling process, microstructural control of the inner oxide layer to eliminate its detrimental effect is necessary.

In this study, the change in microstructure of the outer and inner layers formed on Fe-5 mass%Ni alloy during oxidation is investigated. In particular, the change in the microstructure of the metal particles in the inner layer with oxidation time is considered.

The inner layer consisted of FeO, Ni(Fe), and voids. The concentration of Ni in the Ni(Fe) was found to increase across the inner layer from the scale/steel interface toward the outer/inner scale interface due to the equilibrium Ni concentration in the Ni(Fe) particles with FeO, which corresponded to the oxygen potential gradient in the inner layers. The number and area fraction of the Ni(Fe) metal particles decreased, whereas the size of the particles increased with oxidation time. This coarsening of the metal particles was proposed to be due to Ostwald ripening.

KEY WORDS: oxidation; scale; inner layer; nickel; void; oxygen potential gradient; Ostwald ripening.

1. Introduction

Steel products require a high surface quality as well as characteristics suitable for their intended use. In the hot-rolling processes used in the steel industry, oxide scales formed on the surface of steel exert important effects on the surface quality of the steel products. The scales are usually removed through high-pressure hydraulic descaling prior to the hot-rolling. If the descaling is insufficient, the scales are pushed into the steel, causing surface defects and a poor appearance. Therefore, controlling the microstructure of the scales is important in improving the surface quality of steel products.

Ni containing steels (about 0.5 to 40 mass%) are widely used for various structural components in order to improve low temperature toughness and corrosion resistance. However, removing an oxide scale formed during hot-rolling process on the Ni containing steel by high-pressure hydraulic descaling is known to be difficult.[1–4)] Asai *et al*.[3)] evaluated the removability of scale in Ni containing steel. They reported that the scale becomes difficult to be removed if Ni concentration in the steel is as little as 0.05 mass%. Furthermore, with increasing Ni concentration, it becomes more difficult.

Ni containing steels are known to form a complex structured oxide scale, which consists of an outer layer of Fe-oxides, and an inner layer of the mixture of FeO and Ni(Fe) particles with a complex distribution. This inner oxide scale formation is believed to cause descaling of an oxide scale difficult. Fukagawa *et al*.[5)] proposed a model for the formation of a complex and uneven scale/steel interface in Ni containing steel. During an oxidation of Ni containing steel, an outer layer grows by the outward diffusion of Fe, whereas an inner layer grows by the inward diffusion of oxygen. Below the inner layer, Fe is internally oxidized in the subsurface region because Fe forms much stable oxide, FeO compared to NiO, causing Ni enrichment around them. Ni enrichment also occurs at the scale/steel interface. As oxidation proceeds, the inner layer grows inwardly, and Ni-enriched area and FeO are simultaneously connected to and incorporated in the inner layer, forming an uneven scale/steel interface. Fukagawa *et al*.[6)] also investigated the effects of Ni on the formation of red scales in Si containing steel, and revealed that higher Ni concentration in the steel results in formation of an uneven interface between the eutectic $FeO–Fe_2SiO_4$ compound and steel substrate. In those studies, they proposed the mechanism of the formation of the inner layer as well as the complex scale/steel interface, however, evolution of the microstructure of the inner layer

* Corresponding author: E-mail: harashima.7xt.aya@jp.nipponsteel.com
DOI: https://doi.org/10.2355/isijinternational.ISIJINT-2019-252

© 2020 ISIJ

during oxidation was not discussed, even though it is most important to understand for improving the removability of an oxide scale.

In this study, the development of microstructure of inner layer formed in Fe–Ni alloy is investigated. In particular, we focused on change in the microstructure of Ni-enriched metal particles in the inner layer with oxidation time.

2. Experimental

Fe-5 mass%Ni alloy was prepared by melting the pure constituent metals, Fe (99.95% pure) and Ni (99.99% pure). The chemical composition of the material is shown in **Table 1**. The oxidation samples in size of 30 mm × 30 mm × 3 mm were cut from the ingots and their surfaces were polished. Oxidation was performed in an infrared heating furnace. The samples were heated up to 1 200°C for 5 min in an atmosphere of N_2, and held at 1 200°C for 1, 5, 15, 30, and 60 min in an atmosphere of 10%O_2-20%H_2O-bal.N_2, and then cooled to room temperature in an atmosphere of N_2. Flow rates of the gases were adjusted to 3 L/min. During heating, the oxidation behavior was investigated by measuring the mass gain of the samples using thermogravimetric analysis. The cross-sectional microstructures of the samples after oxidation were observed using optical microscopy. The thicknesses of the scales were measured from their cross-sectional microstructures. The concentration profiles of Fe, Ni, and O in the scales were measured using EPMA. Change in the number, size, and area fraction of Ni(Fe) precipitates along a thickness of the inner layer were obtained from the cross-sectional optical microstructures by image analysis. In this analysis, the inner layer was divided into equal areas in thickness direction at intervals of 15 μm, and each Ni(Fe) metal precipitate is treated as an independent particle. Although the quantitative evaluation of Ni(Fe) precipitates was performed on various views and divisions of the inner layer, a certain result of the quantitative evaluation of Ni(Fe) precipitates will be referred as cross-sectional microstructures of the inner layer are uniform on each sample.

3. Results

3.1. Oxidation Kinetics and Whole Scale Microstructure

The oxidation kinetics of Fe-5 mass%Ni alloys in 10%O_2-20%H_2O-bal.N_2 at 1 200°C is shown in **Fig. 1**. The oxidation proceeded rapidly and did not follow the parabolic behavior. The cross-sectional microstructures of the scales in Fe-5 mass%Ni alloys after different oxidation time are shown in **Fig. 2**. Duplex oxide scales with the outer and inner layers were formed after all oxidation time. The outer layer consisted of multilayered structure with Fe_2O_3, Fe_3O_4, and $FeO+Fe_3O_4$ in this order from the surface. Relatively large voids, in dark contrast, were observed in the outer layer.

Table 1. Chemical composition of the sample (mass%).

C	Ni	Si	Mn	P	S	Al	N
0.011	5.03	<0.003	<0.003	<0.002	<0.0003	<0.002	0.0018

A magnified view of the inner layers is shown in **Fig. 3**. The inner layer consisted of FeO and Ni(Fe) metal particles with bright contrast. Different size and shape of voids, which are seen in darkest contrast, were distributed in the inner layer. The scale/steel interface was uneven due to the penetration of needle-like FeO into the steel substrate.

The thicknesses of the outer and inner layers as a function of oxidation time measured from the cross-sectional microstructures are shown in **Fig. 4**. Each layer was found to grow linearly with oxidation time.

3.2. Voids and Ni(Fe) Metal Particles in the Scales

Large cavities/voids were observed in the outer layer and were aligned each other parallel to the steel surface to form a gap in the outer oxide layer. The aligned voids structure was also observed in the inner oxide layer. The size of the voids in the inner layer decreased as they approached the scale/steel interface. Many voids were observed in the inner layer. The shape of the voids formed near this interface was needle-like, and they formed along a needle-like Ni(Fe) particles. This needle-like voids formation was prone to form near the scale/steel interface.

As shown in Fig. 3, the morphology of the metal particles was found to change from a complex plate-like or needle-like shape near the inner/steel interface to be circular at the outer/inner interface. **Figure 5** shows (a) the number in the unit area, (b) the mean particle size, and (c) the area fraction of the Ni(Fe) metal particles in the inner layer as a function of the distance from the outer/inner interface. The number of the metal particles increased from the outer/inner interface toward the scale/steel interface, but it decreased with oxidation time as shown in Fig. 5(a). However, the mean size of the particles in all inner layers formed after different oxidation time rapidly decreased near the outer/inner interface, and it gradually decreased toward the scale/steel interface as shown in Fig. 5(b). The size of the particles was also confirmed to increase with oxidation time. The area fraction, which represents the product of the number and size, increased gradually from the outer/inner interface and rapidly increased near the scale/steel interface as shown in Fig. 5(c). The area fraction of the particles formed after different oxidation time was almost the same near the outer/

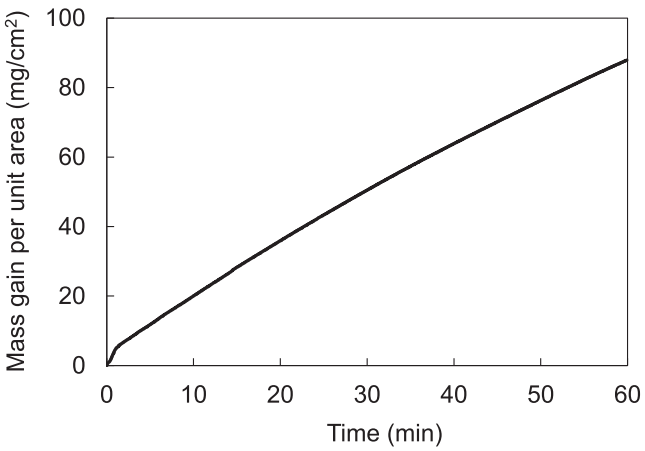


Fig. 1. Oxidation kinetics of Fe-5 mass%Ni alloy oxidized at 1 200°C in 10%O_2-20%H_2O-bal.N_2 for 60 min, plotted with time.

© 2020 ISIJ

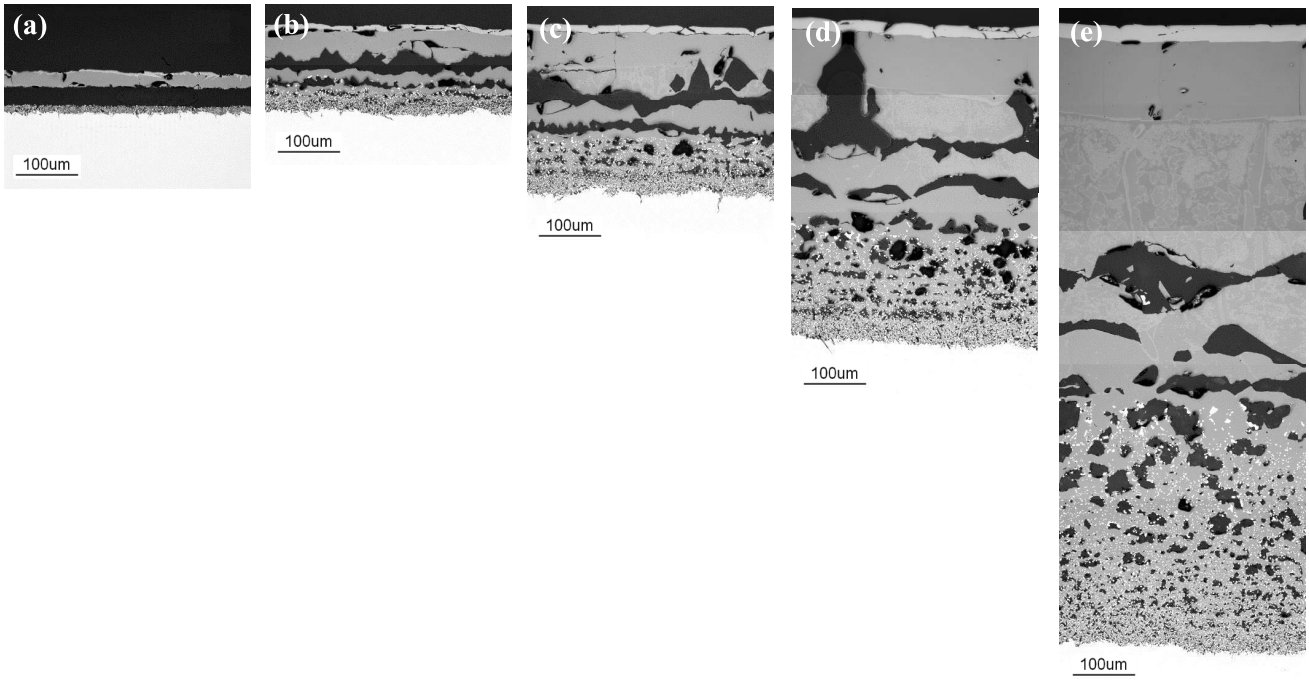


Fig. 2. Cross-sectional microstructures of Fe-5 mass%Ni alloy oxidized at 1 200°C in 10%O_2-20%H_2O-bal.N_2 for (a) 1, (b) 5, (c) 15, (d) 30, and (e) 60 min.

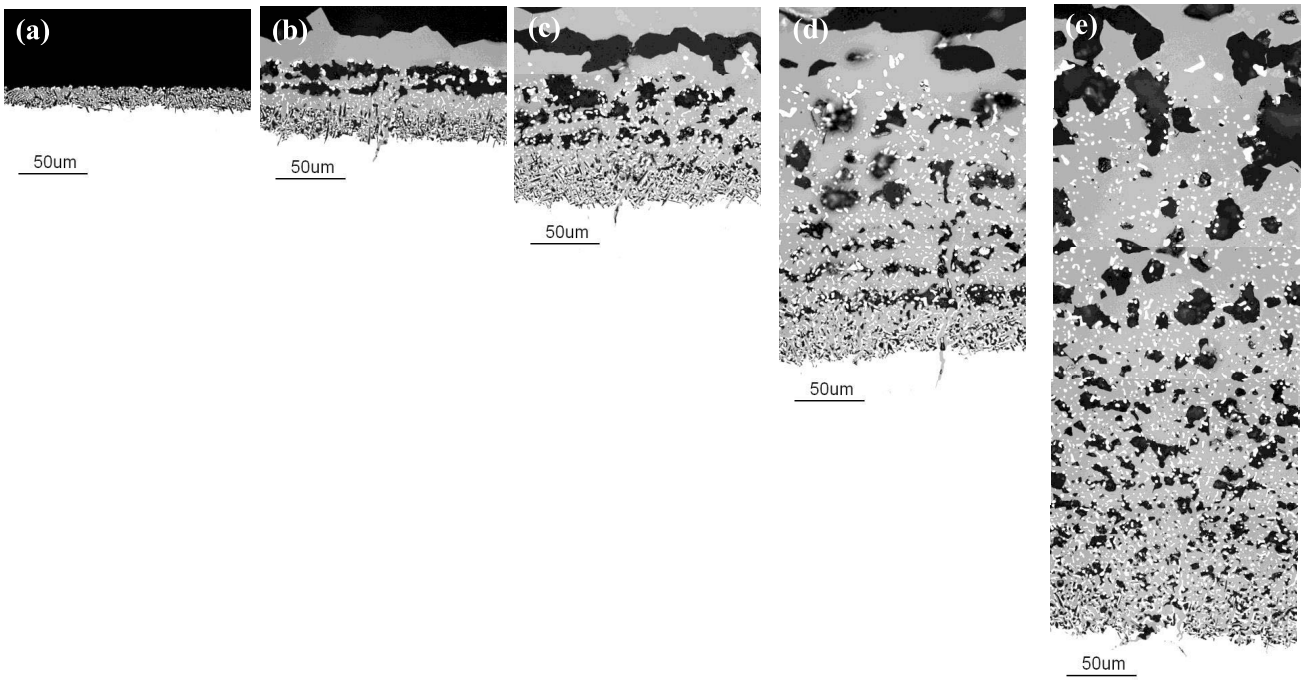


Fig. 3. Higher magnification images of the inner scale of Fe-5 mass%Ni alloy oxidized at 1 200°C in 10%O_2-20%H_2O-bal.N_2 for (a) 1, (b) 5, (c) 15, (d) 30, and (e) 60 min.

inner interface, but it tended to decrease with oxidation time near the scale/steel interface. As we will discuss below, the size and area fraction of Ni(Fe) particles depends on not only oxidation time but also oxygen potential, since those can be a function of Ni contents in Ni(Fe) particles with the assumption of Ni is not oxidized, and Ni contents in Ni(Fe) particles varies with the depth position in the inner layer depending on the oxygen potential across the inner layer. Namely, size of Ni(Fe) particles can be reduced by consumption of Fe at outer/inner interface where the oxygen potential is high. **Figure 6** shows the rearranged plots of Fig. 5. In Fig. 6, the distance from the outer/inner interface is normalized to total thickness of the inner layer in order to observe the effect of oxidation time on the change of the metal particles. Figure 6 indicates that the metal particles became larger with oxidation time, in particular near the outer/inner interface and number of precipitates decreased with oxidation time, which indicate coarsening of the particles.

© 2020 ISIJ

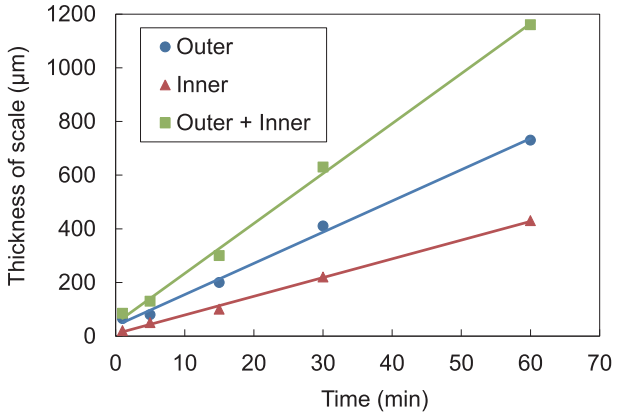


Fig. 4. Thickness of each layer of scales formed on Fe-5 mass%Ni alloy oxidized at 1 200°C in 10%O_2-20%H_2O-bal.N_2.

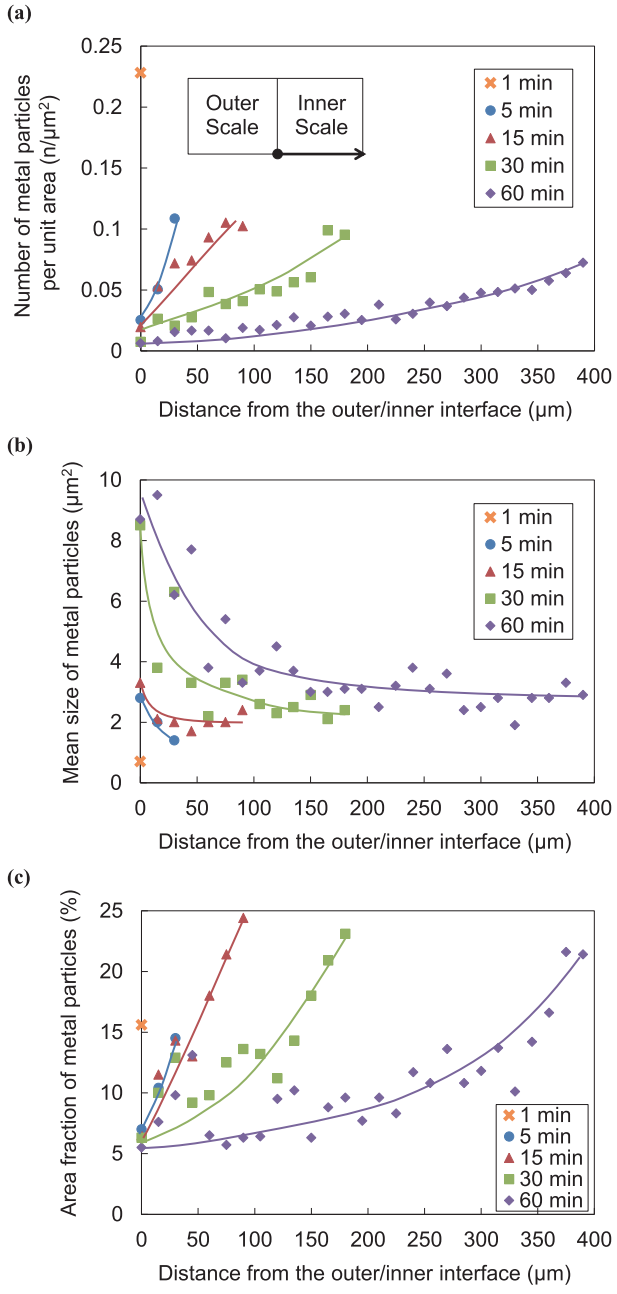


Fig. 5. Plots of (a) number, (b) mean size, and (c) area fraction of metal particles with distance from the interface between outer/inner layer for Fe-5 mass%Ni alloy oxidized at 1 200°C in 10%O_2-20%H_2O-bal.N_2.

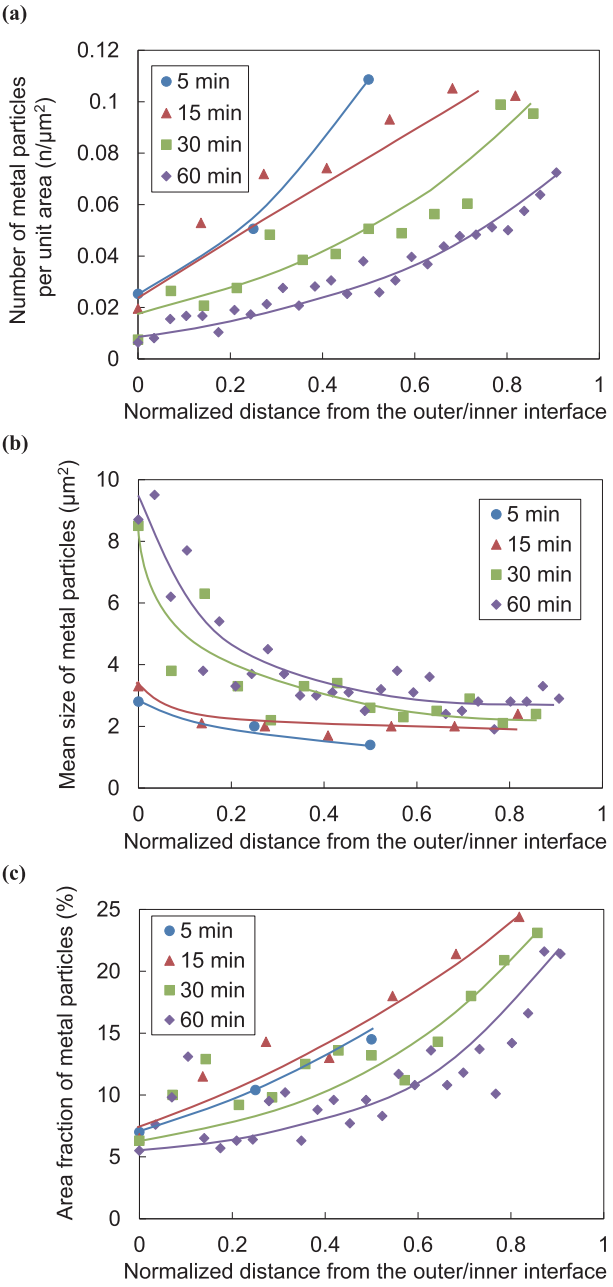


Fig. 6. Plots of (a) number, (b) mean size, and (c) area fraction of metal particles with normalized distance from the interface between outer/inner layer for Fe-5mass%Ni alloy oxidized at 1 200°C in 10%O_2-20%H_2O-bal.N_2.

3.3. Concentration Profiles of the Elements

The distribution of each element in Fe-5 mass%Ni alloys oxidized for 30 and 60 min obtained by EPMA is shown in **Figs. 7** and **8**. As mentioned above, Ni was not found in the outer layer, but accumulated in the inner layer. As shown in the previous section, Ni detected in the inner layer implies the concentration of Ni in the metal particles. Although the size of the metal particles was too small to obtain the concentration of Ni in the particles accurately, the concentration of Ni near the scale/steel interface was similar to that of the alloy, about 5 mass%, and it increased toward the outer/inner interface. The maximum concentration of Ni reached approximately 50 mass% near the outer/inner interface after oxidation for 30 min, whereas it was found to increase approximately 60 mass% after oxidation for 60 min.

© 2020 ISIJ

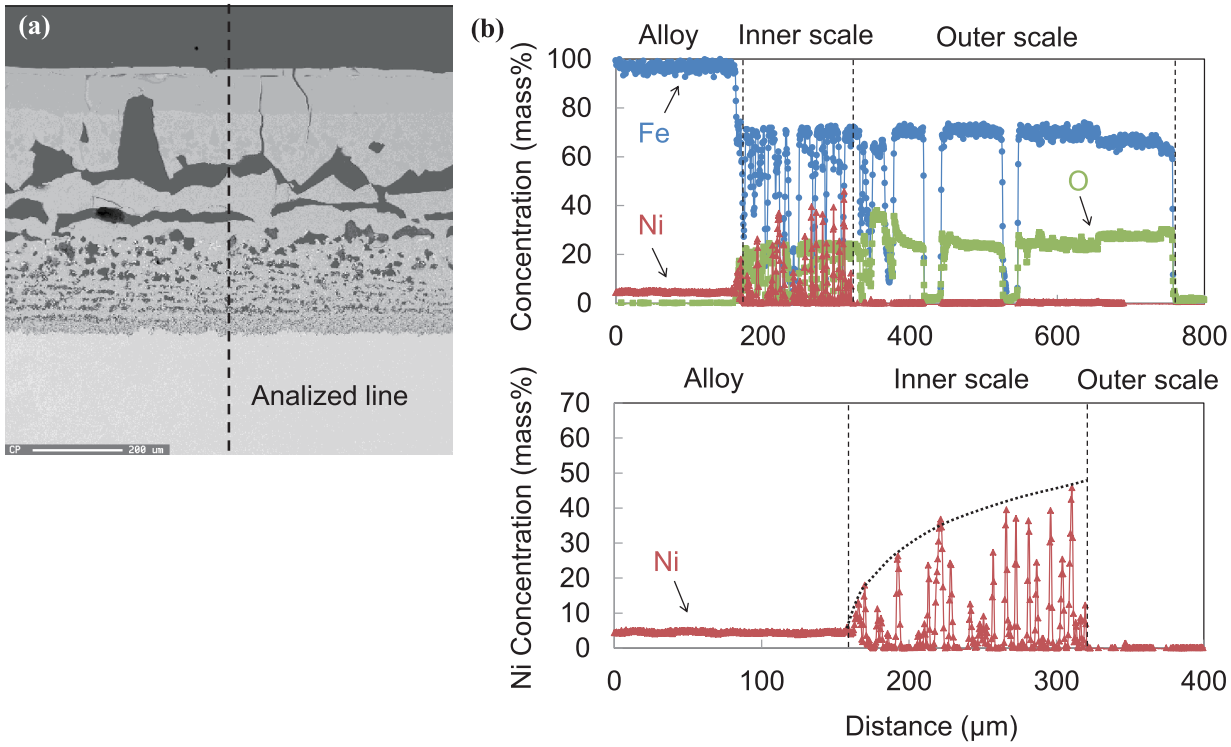


Fig. 7. (a) BEI cross-sectional microstructure and (b) concentration profiles of Fe, Ni, and O of Fe-5 mass%Ni alloy oxidized at 1 200°C in 10%O_2-20%H_2O-bal.N_2 for 30 min.

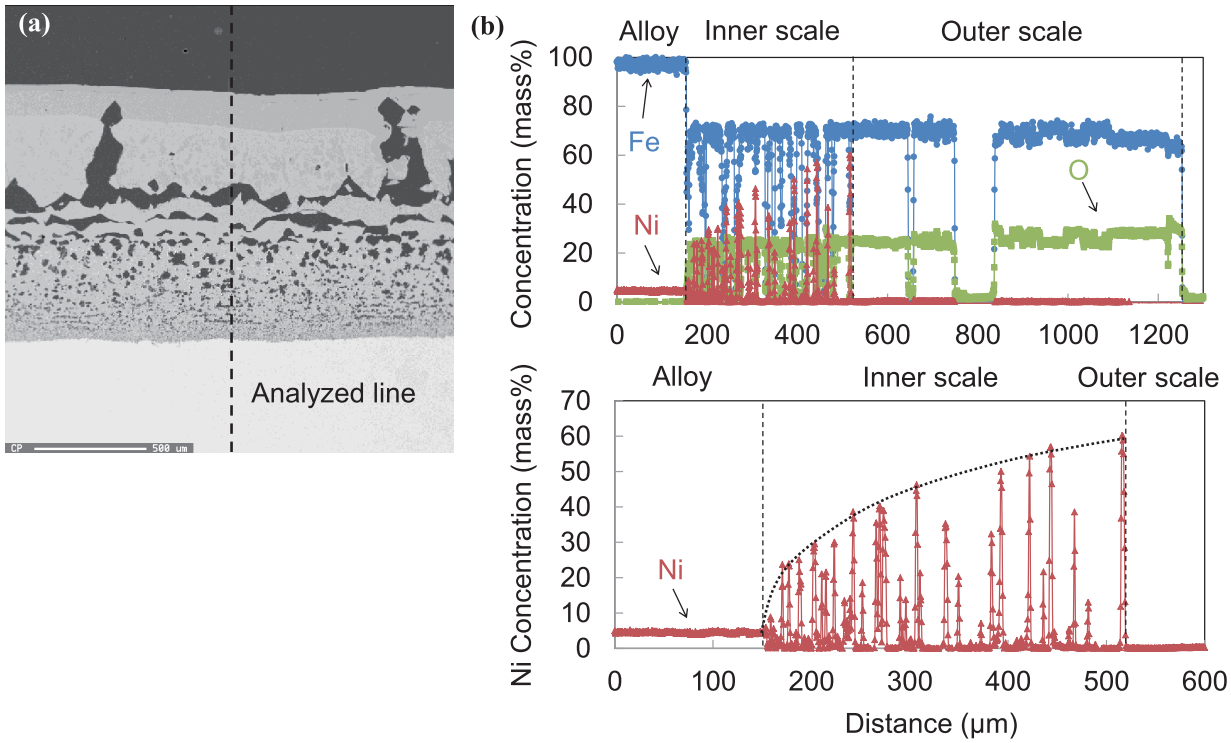


Fig. 8. (a) BEI cross-sectional microstructure and (b) concentration profiles of Fe, Ni, and O of Fe-5 mass%Ni alloy oxidized at 1 200°C in 10%O_2-20%H_2O-bal.N_2 for 60 min.

4. Discussion

Oxidation kinetics of Fe-5 mass%Ni alloy at 1 200°C in 10%O_2-20%H_2O-bal.N_2 did not show the parabolic behavior in the given oxidation time, up to 60 min. There have been a lot of investigations[7–22] about oxidation kinetics of Ni containing steel for various Ni concentration, temperature, atmosphere, and oxidation time, however, most of them reported that oxidation kinetics of Ni containing steel followed parabolic behavior. In this study, the growth of the oxide scale was not only controlled by the mass transport in the oxide scale, but also in the gas boundary layer. Because the samples were heated in flowing N_2 gas during heating and the oxidizing gas was introduced in the reaction cham-

© 2020 ISIJ

ber when temperature reached at 1 200°C in the present study, it takes a longer time to reach the steady-state condition in this study comparing to the condition in which the samples are heated in the oxidizing atmosphere.

Voids were aligned each other parallel to the steel surface in the oxide layer. The size of the voids in the layers decreased as they approach the scale/steel interface, whereas their number increased. Similar porous microstructure of the inner layer was observed in the study of Fe-5 mass% Ni by Fukumoto *et al*.[7] The concentration of Ni near the scale/steel interface was similar to that of the alloy, about 5 mass%, and it increased toward the outer/inner interface. Such behavior was also reported in the study of Fe-5 mass% Ni by Fukumoto *et al*.[7]

The number and area fraction of the metal particles decreased with oxidation time, whereas their size increased. Such change of the metal particles has not been focused on in the previous studies about Ni containing steel.

4.1. Voids in the Oxide Scale

A thick duplex oxide scale has already developed after 1 min of oxidation. Both the outer and inner oxide layer contains large voids/cavities. Such void formation should be caused by a counter diffusion of vacancies due to the outward diffusion of Fe ions across the whole oxide scale and the nucleation of voids in the oxide scale. Ueda *et al*.[23–27] quantitatively estimated the rate of void formation by divergence of ionic flux under an oxygen potential gradient, and could evaluate the void formation behavior in growing oxide scale well. It is reasonable to consider that void nucleation initially occurs heterogeneously at the outer/inner scale interface, and grows laterally to form a gap at the interface based on the cross-sectional observation in Fig. 2(a). Those void arrays in the outer layer are formed in the FeO–Fe_3O_4 two phase region, which would be FeO at 1 200°C during oxidation, indicating that the oxygen potential gradient across the FeO layer changed with oxidation time. Similar void arrays are also observed in the inner layer. The number of the voids formed in the inner layer is larger, whereas the size is smaller than that of the outer layer. The size of the voids tends to be larger at the outer/inner interface and decreases toward the scale/steel interface. Additionally, the size of the voids becomes larger with oxidation time. Since the inner layer grows inwardly,[7,28,29] voids are considered to nucleate near the scale/steel interface and grow larger with oxidation time. As will be discussed later, Ni(Fe) metal particles are incorporated in the inner layer accompanied with the recession of the scale/steel interface. The interface between Ni(Fe) particles and FeO near the scale/steel interface can be a nucleation site of the vacancies.

4.2. Growth of Ni(Fe) Metal Particles

As indicated in Fig. 5(b), the increase in the mean size of the particles with oxidation time is very small near the scale/steel interface, but it becomes larger toward the outer/inner interface. Because the inner layer grows inwardly, the scale/steel interface is oxidation front, and the Ni(Fe) metal particles precipitate at the scale/steel interface. Thus, the size of the particles is independent of oxidation time. However, it is observed that the size of the particles increases and the number of metal particles decreases simultaneously with oxidation time near the outer/inner interface, indicating that the metal particles coarsen during oxidation. Regarding such coarsening of the metal particles, the following two aspects should be considered. First, considering the existence of an oxygen potential gradient in the inner layer, the number, size, and fraction of the metal particles in the inner layer can depend on the oxygen potential gradient across such scales. Consequently, the metal particles can be distributed in the inner layer according to the oxygen potential during oxidation. Second, the metal particles grow due to Ostwald ripening. As shown in Figs. 7 and 8, Ni concentration in the Ni(Fe) particles formed in the inner layer increased toward the outer/inner interface. This is due to the oxygen potential gradient across the inner layer, which consists of FeO–Ni(Fe) two phases. Oxygen potential increases toward the outer/inner interface. As shown in **Fig. 9**,[30] the equilibrium Ni concentration in the Ni(Fe) metal particles with FeO increases with increasing oxygen potential. The area fraction of the Ni(Fe) metal particles embedded in FeO in the inner layer should decrease toward the outer/inner interface from the scale/steel interface by Fe rejection from the metal particles to FeO to maintain the equilibrium condition as shown in Figs. 5(c) and 6(c). Moreover, if the number, size, and area fraction of the metal particles in the inner layer depend solely on the oxygen potential, all the normalized plots at different time as shown in Fig. 6 must be same. However, the plots are not same. Moreover, the size of the metal particles increased even though they should be smaller toward the surface as Fe is rejected from the Ni(Fe) metal particles to FeO in order to maintain the equilibrium condition, however, the size of the metal particles increased where the same oxygen potential is maintained at the same normalized distance from the outer/inner interface. These results strongly indicate that the metal particles coarsened with oxidation time by Ostwald ripening.

Ostwald ripening regarding coarsening of the precipitates in an alloy is represented through Eq. (1).[31,32]

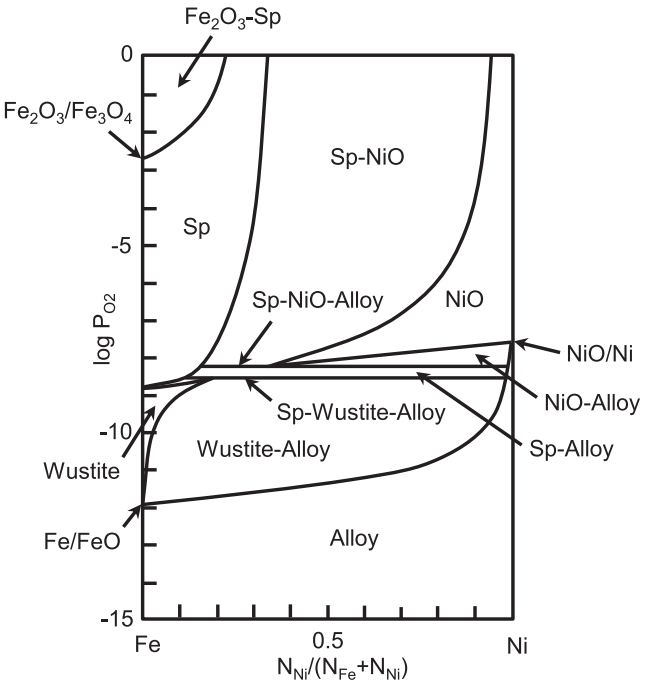


Fig. 9. The Fe–Ni–O ternary system at 1 200°C.[30]

© 2020 ISIJ

$$\bar{r}^3 - \bar{r}_0^3 = K \times t \quad \text{..... (1)}$$

Here, $\bar{r}$ and $\bar{r}_0$ are the mean radii at time t ($t>0$) and $t=0$, and K is constant. For simplicity, assuming $\bar{r} \gg \bar{r}_0$, and taking the logarithm of both sides of Eq. (1), Eq. (2) can be obtained.

$$\ln(r) = \frac{1}{3}\ln(t) + K' \quad \text{..... (2)}$$

Here, K' is constant. Focusing on the size of the metal particles near the outer/inner interface obtained in this experiment, the change in the radii of the metal particles with time can be evaluated under the assumption that the metal particles are spherical in shape. The logarithmic plots for the change with time are shown in **Fig. 10**. In order to obtain sufficient data points, only the results at x = 0, 15, and 30 μm for the outer/inner interface were evaluated. The data points are scattered, however, slopes of the graph at x = 0, 15, and 30 μm for this interface are 0.31, 0.30, and 0.34, respectively, which agree with the value of 1/3 shown in Eq. (2), indicating that the metal particles become coarser by Ostwald ripening. As mentioned above, since the size of the metal particle may depend on oxygen potential, the plots obtained from 15 and 30 μm for the outer/inner interface could be less accurate, however, the influence of the oxygen potential can be neglected at the outer/inner interface, *i.e.*, 0 μm position. With the coarsening by Ostwald ripening, the area fraction of the metal particles in the inner layer must be constant across the inner layer. However, it increased toward the scale/steel interface. This can be due to Fe rejection from the Ni(Fe) particles by rearrangement of the oxygen potential gradient accompanied with the growth of the oxide scale. Formation of voids and its growth in the inner layer would also influence the evaluation of the area fraction of the metal particles and the normalized distance of the inner layer.

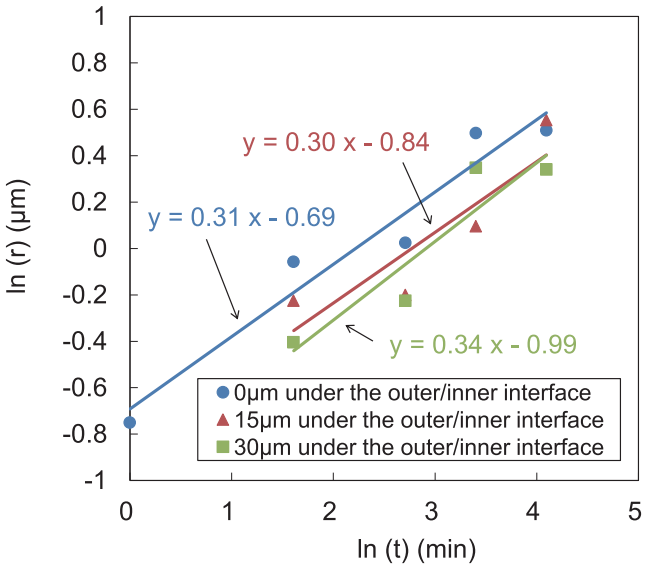


Fig. 10. Logarithmic plots of radius of metal particles with time for Fe-5 mass%Ni alloy oxidized at 1 200°C in 10%O_2-20%H_2O-bal. N_2.

5. Conclusion

Fe-5 mass%Ni alloys were oxidized at 1 200°C in an atmosphere of 10%O_2-20%H_2O-bal.N_2, and the change in microstructure of oxide scale with time was investigated. The following conclusions are drawn:

(1) Duplex oxide scales with the outer and inner layers were formed. FeO, Ni(Fe) metal particles, and voids were observed in the inner layers.

(2) Voids were aligned each other parallel to the steel surface in the oxide scale. The size of the voids in the scale decreased as they approach the scale/steel interface.

(3) The concentration of Ni in the metal particles increased from the outer/inner interface toward the scale/steel interface corresponding to the oxygen potential gradient across the inner layer.

(4) The number and the area fraction of metal particles decreased with oxidation time, whereas their size increased. The metal particles were found to grow with oxidation time due to Ostwald ripening.

REFERENCES

1) T. Asai, T. Soshiroda and M. Miyahara: *ISIJ Int.*, **37** (1997), 272.
2) W. Melfo, H. Bolt, M. Rijnders, D. Staalman, C. B. Castro, D. Crowther and B. Jana: *ISIJ Int.*, **53** (2013), 866.
3) Y. Z. Liu, C. F. Yang, F. Chai, T. Pan and H. Su: *J. Iron Steel Res. Int.*, **21** (2014), 956.
4) Y. N. Chang: *China Steel Tech. Rep.*, **21** (2008), 52.
5) T. Fukagawa and H. Fujikawa: *Oxid. Met.*, **52** (1999), 177.
6) T. Fukagawa, H. Okada, Y. Maehara and H. Fujikawa: *Tetsu-to-Hagané*, **82** (1996), 63 (in Japanese).
7) M. Fukumoto, S. Hayashi, S. Maeda and T. Narita: *J. Jpn. Inst. Met.*, **66** (2002), 513 (in Japanese).
8) R. T. Foley, J. U. Druck and R. E. Fryxell: *J. Electrochem. Soc.*, **102** (1955), 440.
9) I. A. Menzies and W. J. Tomlinson: *J. Iron Steel Inst.*, **204** (1966), 1239.
10) L. A. Morris and W. W. Smeltzer: *Acta Metall.*, **15** (1967), 1591.
11) G. G. Brown and K. G. Wold: *J. Iron Steel Inst.*, **207** (1969), 1457.
12) T. J. Carter, G. L. Wulf and G. R. Wallwork: *Corros. Sci.*, **9** (1969), 471.
13) A. D. Dalvi and W. W. Smeltzer: *J. Electrochem. Soc.*, **118** (1971), 1978.
14) F. Matsuno, S. Nishikida and T. Harada: *Tetsu-to-Hagané*, **67** (1981), 2029 (in Japanese).
15) F. Matsuno and S. Nishikida: *Tetsu-to-Hagané*, **68** (1982), 301 (in Japanese).
16) K. Kusabiraki, H. Toki, T. Ishiguro and T. Ooka: *Tetsu-to-Hagané*, **74** (1988), 871 (in Japanese).
17) S. Ando and H. Kimura: *Metall. Trans. A*, **22** (1991), 2393.
18) T. Kato, M. Kawamoto and T. Watanabe: *Tetsu-to-Hagané*, **82** (1996), 564 (in Japanese).
19) K. Kusabiraki, K. Sakuradani and S. Saji: *Tetsu-to-Hagané*, **84** (1998), 291 (in Japanese).
20) X. Guo, K. Kusabiraki and S. Saji: *Oxid. Met.*, **58** (2002), 589.
21) T. Inoue, A. Kobayashi, K. Yamauchi and Y. Hosoya: *Tetsu-to-Hagané*, **93** (2007), 409 (in Japanese).
22) J. Y. Yun, D. H. Park, D. W. Lee, S. M. Shin, Y. H. Kim and J. P. Wang: *Journal of Electrical Engineering*, **2** (2014), 49.
23) M. Ueda, K. Kawamura and T. Maruyama: *Mater. Sci. Forum*, **522–523** (2006), 37.
24) T. Maruyama, K. Akiba, M. Ueda and K. Kawamura: *Mater. Sci. Forum*, **595–598** (2008), 1039.
25) T. Maruyama, M. Ueda and K. Kawamura: *Defect Diffus. Forum*, **289–292** (2009), 1.
26) T. Maruyama and M. Ueda: *J. Korean Ceram. Soc.*, **47** (2010), 8.
27) M. Ueda, K. Kawamura and T. Maruyama: *Mater. Sci. Forum*, **696** (2011), 34.
28) M. Fukumoto, S. Maeda, S. Hayashi and T. Narita: *Tetsu-to-Hagané*, **86** (2000), 526 (in Japanese).
29) M. Fukumoto, S. Maeda, S. Hayashi and T. Narita: *Oxid. Met.*, **55** (2001), 401.
30) M. A. Rhamdhani, P. C. Hayes and E. Jak: *Metall. Mater. Trans. B*, **39** (2008), 690.
31) I. M. Lifshitz and V. V. Slyozov: *J. Phys. Chem. Solids*, **19** (1961), 35.
32) C. Wagner: *Z. Elektrochem.*, **65** (1961), 581.

© 2020 ISIJ